

Reducing molecular electronic Hamiltonian simulation cost for Linear Combination of Unitaries approaches

Ignacio Loaiza,^{1,2} Alireza Marefat Khah,^{1,2} Nathan Wiebe,^{3,4} and Artur F. Izmaylov^{1,2}

¹⁾*Chemical Physics Theory Group, Department of Chemistry, University of Toronto, Toronto, Canada*

²⁾*Department of Physical and Environmental Sciences, University of Toronto Scarborough, Toronto, Canada*

³⁾*Department of Computer Science, University of Toronto, Toronto, Canada*

⁴⁾*Pacific Northwest National Laboratory, Richland, USA*

(Dated: 18 August 2022)

We consider different linear combination of unitaries (LCU) decompositions for molecular electronic structure Hamiltonians. Using these LCU decompositions for Hamiltonian simulation on a quantum computer, the main figure of merit is the 1-norm of their coefficients, which is associated with the quantum circuit complexity. It is derived that the lowest possible LCU 1-norm for a given Hamiltonian is half of its spectral range. This lowest norm decomposition is practically unattainable for general Hamiltonians; therefore, multiple practical techniques to generate LCU decompositions are proposed and assessed. A technique using symmetries to reduce the 1-norm further is also introduced. In addition to considering LCU in the Schrödinger picture, we extend it to the interaction picture, which substantially further reduces the 1-norm.

I. INTRODUCTION

Quantum chemistry is often regarded as one of the most promising applications for quantum computers. The number of qubits required to represent the electronic states of a molecular Hamiltonian scales linearly with the number of orbitals, whereas an exponentially large number of classical bits is required; this is commonly known as the curse of dimensionality. In addition to be able to record the quantum wavefunction one needs to be able to prepare it. Over the last years, several quantum algorithms for efficient eigenstate state preparation have appeared, such as Quantum Phase Estimation^{1,2}. These algorithms require an implementation of the dynamical evolution operator $e^{-i\hat{H}t}$ and the electronic structure Hamiltonian³

$$\hat{H} = \sum_{\sigma=\{\alpha,\beta\}} \sum_{ij}^N \tilde{h}_{ij} \hat{E}_{j\sigma}^{i\sigma} + \sum_{\sigma,\sigma'=\{\alpha,\beta\}} \sum_{ijkl}^N \tilde{g}_{ijkl} \hat{E}_{j\sigma}^{i\sigma} \hat{E}_{l\sigma'}^{k\sigma'}, \quad (1)$$

where $\{\sigma, \sigma'\}$ are spin- z projections, $\{i, j, k, l\}$ are spacial orbitals, \tilde{h}_{ij} and \tilde{g}_{ijkl} are one- and two-electron integrals⁴, and $\hat{E}_q^p \equiv \hat{a}_p^\dagger \hat{a}_q$ are single excitation operators (here and for the remainder of this work, we use the indices $\{p, q, r, s\}$ to refer to spin-orbitals).

Implementing the time-evolution operator is a non-trivial task, known as the Hamiltonian simulation problem. This is usually done by decomposing the Hamiltonian into parts with favorable properties (e.g. fast-forwardable, unitary), in approaches based on 1) Lie-Trotter-Suzuki formulas⁵, 2) qubitization^{6–8}, 3) Dyson series⁹, and 4) qDRIFT^{8,10,11}. In all of these approaches, the decomposition method, together with the simulation method, define the necessary quantum resources for the simulation (i.e. number of gates and logical qubits). Some approaches, such as those based on a Lie-Trotter-Suzuki expansion, do not require additional an-

cilla qubits, but can require significantly deeper circuits to achieve the same worst-case error bounds for non-local Hamiltonians^{12,13}, whereas the tensor hypercontraction decomposition with a qubitization simulation yields the best gate provable complexity scaling to the best of our knowledge⁸.

Even though the quantum cost of realizing the time-evolution operator has a complicated dependence such as the decomposition that is being used and the particular implementation of the simulation algorithm, the gate complexity of qubitization, LCU and QDrift can be shown to scale with respect to the 1-norm of the Hamiltonian decomposition into a linear combination of unitaries (LCU)^{9,14,15} $\hat{H} = \sum_k u_k \hat{U}_k$, namely $\sum_k |u_k|$. Thus minimizing this 1-norm of coefficients is vital for reducing the costs of a quantum simulation.

In this work, we focus on ways to decompose and transform the Hamiltonian such that the resulting 1-norm is minimized. We propose three approaches that can be used for lowering the 1-norm. The first builds the LCU's unitaries by grouping mutually anti-commuting Pauli products in the Hamiltonian after doing the fermion to qubit mapping¹⁶, which either maintains or lowers the 1-norm. The second approach shifts the Hamiltonian by using symmetry operators. Both of these approaches are of interest for any method which decomposes the Hamiltonian as a LCU. The third approach makes use of the interaction picture algorithm¹⁴ combined with a LCU decomposition. The basic idea is to separate the Hamiltonian into two fragments: a main one with an exponential that is straightforward to calculate, and a residual with a significantly smaller 1-norm. The Hamiltonian simulation is then performed by rotating the residual to the interaction picture frame. Simulating the residual, as shown in Ref. 14, will generally have a significantly lower cost than the full Hamiltonian simulation. The only caveat is that the residual becomes time-dependent

in this new frame, requiring a time-dependent simulation method. Since only time-independent Hamiltonians can be simulated through qubitization, we use the Dyson series approach, which can also be used for time-dependent simulations while presenting an almost optimal scaling with respect to the 1-norm and simulation time^{9,14}. It is worth noting though that other approaches such as QDrift that has 1-norm scaling will also benefit from these optimizations¹⁷.

This rest of the paper is organized as follows. We start by reviewing the Dyson series simulation method in Sec. II A. A 1-norm lower bound theorem for LCU decompositions is then given in Sec. II B, followed by an overview of different LCU decomposition strategies in Sec. II C. A general methodology for reducing the simulation cost by using symmetries is shown in Sec. II D. Section II E reviews the essential elements of the interaction picture method¹⁴, along with our procedure for partitioning the Hamiltonian into two fragments. Once all the necessary methodologies have been introduced, our numerical results along with their discussion are shown in Sec. III.

II. THEORY

A. Hamiltonian simulation by LCU decomposition

An LCU decomposition for a Hamiltonian can be written as

$$\hat{H} = \gamma \hat{1} + \sum_k u_k \hat{U}_k, \quad (2)$$

where u_k 's are generally complex numbers, and \hat{U}_k 's are unitary operators. The identity shift can be trivially added or removed as a phase since $e^{-i(\hat{H} + \gamma \hat{1})t} = e^{-i\hat{H}t} e^{-i\gamma t \hat{1}}$, while still affecting the spectral norm of the Hamiltonian. The LCU in Eq.(2) has an associated 1-norm for coefficients of nontrivial unitaries

$$\lambda = \sum_k |u_k|. \quad (3)$$

The LCU decomposition allows one to construct a Hamiltonian oracle, a circuit that, with the usage of some ancilla qubits, is able to encode the action of \hat{H} on an arbitrary function $|\psi\rangle$. As shown in Fig. 1, the output of the oracle circuit contains a spurious remainder, which is made arbitrarily small through the subsequent use of amplitude amplification. The time-evolution operator $e^{-i\hat{H}t}$ can always be expanded as a series: this expansion is known as a Dyson series, which reduces to a Taylor series for the case where \hat{H} is time-independent. $e^{-i\hat{H}t}$ is thus realized up to an arbitrary error ϵ by implementing a truncated Dyson series using the amplitude amplified oracle circuit^{9,14,18}.

The cost of performing the Hamiltonian simulation with an error bound ϵ scales in a linear, or nearly linear,

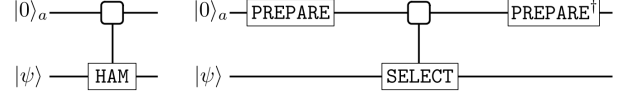


FIG. 1. Arbitrary Hamiltonian oracle (left) and LCU oracle (right) implementation by block-encoding, both with output $|0\rangle_a \otimes \frac{\hat{H}}{\lambda} |\psi\rangle + |\text{remainder}\rangle$. $\text{PREPARE}|0\rangle_a = \sum_k \sqrt{\frac{u_k}{\lambda}} |k\rangle_a$ and $\text{SELECT} = \sum_k |k\rangle_a \langle k|_a \otimes \hat{U}_k$ for the LCU shown in Eq.(2) and $|k\rangle_a$ the k -th state of the ancilla register, requiring $\lceil \log_2 M \rceil$ ancilla qubits, where M is the total number of unitaries in the LCU.

manner with respect to the LCU's 1-norm¹⁴, requiring

$$\mathcal{O}\left(\lambda t \text{ polylog} \frac{\lambda t}{\epsilon}\right) \quad (4)$$

applications of the oracle circuit for truncated Dyson simulation methods or

$$\mathcal{O}\left(\lambda t + \text{polylog} \frac{1}{\epsilon}\right), \quad (5)$$

using qubitization^{19,20}. The main aim of this work is to explore different ways in which we can reduce the 1-norm λ , lowering the quantum circuit depth/complexity of the Hamiltonian simulation.

B. 1-norm bound

Let us start with a few general remarks on the minimum possible 1-norm and approaches for its minimization in practical LCU procedures for the electronic Hamiltonian.

Theorem 1 (1-norm bound). *For a bounded hermitian operator \hat{H} , all its possible LCU decompositions have an associated 1-norm which is lower bounded by $\Delta E/2 \equiv (E_{\max} - E_{\min})/2$, where $E_{\max}(E_{\min})$ is the highest (lowest) eigenvalue of \hat{H} .*

Formal proof of the theorem is given in Appendix A. A construction that achieves the minimum 1-norm follows from the following sequence of steps:

1. shift the Hamiltonian so that the largest and lowest eigenvalues become $\pm(E_{\max} - E_{\min})/2$:

$$\hat{H}_s = \hat{H} - \left(\frac{E_{\max} + E_{\min}}{2}\right) \hat{1} \quad (6)$$

2. obtain a rescaled Hamiltonian \hat{H}_{sr} such that $\|\hat{H}_{sr}\| = 1$ (where $\|\cdot\|$ is the spectral norm):

$$\hat{H}_{sr} = \frac{2\hat{H}_s}{E_{\max} - E_{\min}} \quad (7)$$

3. form the pair of unitaries:

$$\hat{U}_{\pm} = \hat{H}_{sr} \pm i\sqrt{\hat{1} - \hat{H}_{sr}^2}. \quad (8)$$

This procedure gives the LCU

$$\hat{H} = \left(E_{\min} + \frac{\Delta E}{2}\right) \hat{1} + \frac{\Delta E}{4} (\hat{U}_+ + \hat{U}_-), \quad (9)$$

with $\Delta E/2$ its corresponding 1-norm.

The main problem of achieving this lowest 1-norm is the practical construction of \hat{U}_{\pm} ; for most molecular Hamiltonians they are highly multi-particle operators because of the square-root in their definitions, and their calculation/implementation requires a complicated quantum singular value transformation to implement²⁰ the square-roots in an interval $\|\hat{H}_{sr}\| \in [0, 1 - \delta]$ for some $\delta > 0$. Still, this theorem gives us a bound on the best achievable value for the 1-norm, which is useful to assess the quality of LCU decompositions.

C. Unitary operators for LCU decompositions

In what follows we consider various practical forms of unitaries \hat{U}_k that appear when one is constructing an LCU representation for the electronic structure Hamiltonian [Eq. (1)].

1. Pauli products

The simplest LCU decomposition uses the qubit representation of the Hamiltonian after it has been transformed from its fermionic representation by using one of the many available mappings (e.g. Jordan-Wigner and Bravyi-Kitaev transformations^{21–24}):

$$\hat{H} = \sum_{k=1}^{N_p} c_k \hat{P}_k, \quad (10)$$

where \hat{P}_k are products of Pauli operators on different qubits, c_k are constants, and N_p is the total number of Pauli products. Since Pauli products are already unitary operators, Eq.(10) defines an LCU decomposition where the 1-norm is given by

$$\lambda^{(P)} = \sum_k |c_k|. \quad (11)$$

$\lambda^{(P)}$ can be related to electron integrals \tilde{h}_{ij} and \tilde{g}_{ijkl} as

$$\begin{aligned} \lambda^{(P)} = & \sum_{ij} |\tilde{h}_{ij}| + 2 \sum_k |\tilde{g}_{ijkk}| + \sum_{i>k, j>l} |\tilde{g}_{ijkl} - \tilde{g}_{ilkj}| \\ & + \frac{1}{2} \sum_{ijkl} |\tilde{g}_{ijkl}|. \end{aligned} \quad (12)$$

This relation is obtained using the Majorana representation for the Hamiltonian (detailed in Appendix B).

One way to improve $\lambda^{(P)}$ is to apply orbital transformations \hat{U}_O

$$\hat{U}_O(\vec{\theta}) = e^{\sum_{i>j} \theta_{ij} \sum_{\sigma} (\hat{E}_{j\sigma}^{i\sigma} - \hat{E}_{i\sigma}^{j\sigma})} \quad (13)$$

before transforming the Hamiltonian to qubit or Majorana representation¹⁵, $\hat{U}_O \hat{H} \hat{U}_O^\dagger$. One can optimize the generator coefficients θ_{ij} of orbital rotations in $\hat{U}_O(\vec{\theta})$ with the 1-norm in Eq.(12) as the cost function.

2. Grouping of anti-commuting Pauli products

Another way of reducing 1-norm of the Pauli product decomposition of the Hamiltonian [Eq. (10)] is via grouping of anti-commuting Pauli products¹⁶

$$\hat{H} = \sum_n a_n \hat{A}_n, \quad (14)$$

where

$$a_n = \sqrt{\sum_{i \in K_n} |c_i|^2}, \quad (15)$$

$$\hat{A}_n = \frac{1}{a_n} \sum_{k \in K_n} c_k \hat{P}_k, \quad (16)$$

\hat{A}_n are linear combinations of anti-commuting Pauli products, $\{\hat{P}_k, \hat{P}_{k'}\} = 2\delta_{kk'} \hat{1}$, and $\{K_n\}$ are groups of corresponding indices.

\hat{A}_n are larger unitary transformations, and it can be shown that 1-norm of coefficients in Eq. (14) is always lower or equal than the 1-norm of the initial LCU decomposition: comparison of 1-norms for decompositions in Eqs. (10) and (14)

$$\lambda^{(AC)} = \sum_n |a_n| = \sum_n \sqrt{\sum_{i \in K_n} |c_i|^2} \quad (17)$$

$$\lambda^{(P)} = \sum_k |c_k| = \sum_n \sum_{i \in K_n} |c_i| \quad (18)$$

and using the triangle inequality for each K_n ,

$$\sum_{i \in K_n} |c_i| \geq \sqrt{\sum_{i \in K_n} |c_i|^2}, \quad (19)$$

proves that $\lambda^{(AC)} \leq \lambda^{(P)}$, where the equality takes place only for the trivial case where no grouping is made. Further note that from the Cauchy-Schwarz inequality

$$\sum_{i \in K_n} |c_i| \leq \sqrt{|K_n|} \sqrt{\sum_{i \in K_n} |c_i|^2}, \quad (20)$$

the gulf between these two bounds can be as much as a factor of $\sqrt{|K_n|}$ suggesting that a substantial improvement can be attained in cases where the typical values of $|K_n|$ seen are large.

Once the anti-commuting groups have been found, each unitary \hat{A}_n can be implemented as a product of unitaries:

$$\hat{A}_n = \prod_{k \in K_n \uparrow} e^{i\theta_k \hat{P}_k} \prod_{k \in K_n \downarrow} e^{i\theta_k \hat{P}_k}, \quad (21)$$

where the $\uparrow(\downarrow)$ stands for ascending(descending) through K_n , and

$$\theta_k = \frac{1}{2} \arcsin \frac{c_k}{\sqrt{\sum_{i \in K_n, i \leq k} c_i^2}}. \quad (22)$$

3. Fermionic reflections

One can use fermionic operator algebra to construct an LCU decomposition. It is convenient to start with factorized decomposition of one- and two-electron terms of \hat{H} [Eq. (1)] introduced in double factorization (DF) method^{6,7} and the Cartan subalgebra approach (CSA)²⁵

$$\hat{H}_1 = \sum_{\sigma=\{\alpha,\beta\}} \sum_{ij}^N \tilde{h}_{ij} \hat{E}_{j\sigma}^{i\sigma} \quad (23)$$

$$= \hat{U}_1 \left(\sum_{i\sigma} \lambda_{ii}^{(1)} \hat{n}_{i\sigma} \right) \hat{U}_1^\dagger \quad (24)$$

$$\hat{H}_2 = \sum_{\sigma,\sigma'=\{\alpha,\beta\}} \sum_{ijkl}^N \tilde{g}_{ijkl} \hat{E}_{j\sigma}^{i\sigma} \hat{E}_{l\sigma'}^{k\sigma'} \quad (25)$$

$$= \sum_{m=2}^M \hat{U}_m \left(\sum_{ij,\sigma\sigma'} \lambda_{ij}^{(m)} \hat{n}_{i\sigma} \hat{n}_{j\sigma'} \right) \hat{U}_m^\dagger, \quad (26)$$

where \hat{U}_m are orbital rotations as in Eq. (13), $\hat{n}_p \equiv \hat{E}_p^p$ are the occupation number operators, and $\lambda_{ij}^{(m)}$ are parameters of the decomposition. The difference between DF and CSA decompositions is in the rank of $\lambda_{ij}^{(m)}$, $m > 1$ matrices, DF has $\lambda_{ij}^{(m)} = \epsilon_i^{(m)} \epsilon_j^{(m)}$ as an outer product of $\epsilon_i^{(m)}$ vector, which makes $\text{rank}(\lambda^{(m)}) = 1$, while CSA does not have any restriction on the $\lambda_{ij}^{(m)}$ rank. \hat{H}_2 decompositions are truncated for fragments whose $\lambda_{ij}^{(m)}$ are smaller than some threshold.

The convenience of these decompositions are in simplicity of transforming \hat{n}_p operators into reflections,⁶⁻⁸ $\hat{n}_p \rightarrow (\hat{1} - 2\hat{n}_p) \equiv \hat{r}_p$, where \hat{r}_p is the reflection on spin-orbital p . Accounting for idempotency and hermiticity of \hat{n}_p , one can easily check that $\hat{r}_p^2 = 1$ and $\hat{r}_p^\dagger = \hat{r}_p$. Another important property of \hat{n}_p 's is their commutativity that allows one to transform the two-electron fragment

in LCU

$$\hat{H}_2 \rightarrow \hat{H}_2^{(\text{LCU})} = \sum_{\sigma\sigma'} \sum_m \hat{U}_m \left(\sum_{ij} \frac{\lambda_{ij}^{(m)}}{4} \hat{r}_{i\sigma} \hat{r}_{j\sigma'} \right) \hat{U}_m^\dagger.$$

To use $\hat{H}_2^{(\text{LCU})}$ as a part of the full Hamiltonian, the one-electron part requires the following adjustment

$$\hat{H}'_1 = \hat{H}_1 + 2 \sum_{\sigma} \sum_{ijk} \tilde{g}_{ijk} \hat{E}_{j\sigma}^{i\sigma}. \quad (27)$$

The modified one-electron operator can be decomposed as

$$\hat{H}'_1 = \hat{U}_1 \left(\sum_{\sigma,i} \mu_i \hat{n}_{i\sigma} \right) \hat{U}_1^\dagger, \quad (28)$$

where μ_i are new parameters. Switching $\hat{n}_p \rightarrow \hat{r}_p$ yields up to a constant shift

$$\hat{H}'_1 \rightarrow \hat{H}_1^{(\text{LCU})} = -\hat{U}_1 \left(\sum_{\sigma,i} \frac{\mu_i}{2} \hat{r}_{i\sigma} \right) \hat{U}_1^\dagger. \quad (29)$$

Thus, we have 1-norm $\lambda^{(\text{F})} = \lambda_1 + \lambda_2$ associated with this LCU procedure, where λ_1 (λ_2) is 1-norm of $\hat{H}_1^{(\text{LCU})}$ ($\hat{H}_2^{(\text{LCU})}$)

$$\lambda_1 = \sum_i |\mu_i|, \quad (30)$$

$$\begin{aligned} \lambda_2 &= \frac{1}{4} \sum_m \sum_{\sigma\sigma', ij} |\lambda_{ij}^{(m)}| \\ &= \sum_m \sum_{ij} |\lambda_{ij}^{(m)}| - \frac{1}{2} \sum_m \sum_i |\lambda_{ii}^{(m)}|, \end{aligned} \quad (31)$$

Note that the obtained fermionic LCU decomposition can be transformed to a qubit LCU form using any fermion-qubit mappings.

4. Square-root unitarization technique

Another way to transform the quadratic polynomials

$$\hat{f}^{(m)} = \sum_{ij,\sigma\sigma'} \lambda_{ij}^{(m)} \hat{n}_{i\sigma} \hat{n}_{j\sigma'} \quad (32)$$

into unitaries is via steps described in Theorem 1. This procedure gives the lowest 1-norm for LCU of each fragment. First, we shift and rescale each fragment so that their eigenvalues are in the interval $[-1, 1]$ (i.e. $\hat{f}^{(m)} \rightarrow \hat{f}_{sr}^{(m)}$, as seen in Eqs.(6,7)). Second, unitary operators can be defined for each fragment as

$$\hat{V}_m^{(\pm)} = \hat{f}_{sr}^{(m)} \pm i \sqrt{\hat{1} - (\hat{f}_{sr}^{(m)})^2}. \quad (33)$$

This leads to the LCU of the two-electron Hamiltonian up to a constant as

$$\hat{H}_2^{(\text{LCU})} = \sum_{m=2}^M \frac{\|\hat{f}^{(m)}\|_\Delta}{2} \hat{U}_m (\hat{V}_m^{(+)} + \hat{V}_m^{(-)}) \hat{U}_m^\dagger, \quad (34)$$

where $\|\hat{f}^{(m)}\|_\Delta \equiv f_{\max}^{(m)} - f_{\min}^{(m)}$ is a spectral range of $\hat{f}^{(m)}$ and $f_{\max(\min)}^{(m)}$ is the maximum (minimum) eigenvalue of fragment $\hat{f}^{(m)}$. The corresponding 1-norm is

$$\lambda_2^{(sr)} = \frac{1}{2} \sum_m \|\hat{f}^{(m)}\|_\Delta, \quad (35)$$

In general, the explicit construction and implementation of $\hat{V}_m^{(\pm)}$ unitaries becomes prohibitively expensive as the number of orbitals grows, as the square-root function includes all possible products of the occupation numbers. Using a different scaling such that $\|\hat{f}_{sr}^{(m)}\| \leq 1 - \delta$, this unitary operator can be approximated within error ϵ using $O((\frac{1}{\delta}) \log(1/\epsilon))$ invocations of the fragment $\hat{f}^{(m)20}$. Nevertheless, given the complexity of implementing such circuits, the square-root unitarization is primarily used as a lower bound of the 1-norm for fermionic decompositions.

This procedure can also be done for the one-electron term \hat{H}_1' (Eq.(28)), obtaining

$$\lambda_1^{(sr)} = \left(\sum_{\mu_i > 0} \mu_i - \sum_{\mu_i < 0} \mu_i \right) = \sum_i |\mu_i|. \quad (36)$$

We note that this 1-norm is the same as that in Eq.(30). This shows that, using the fermionic LCU decomposition in Eq. (28) gives the LCU with the lowest possible 1-norm for the one-electron part since its 1-norm coincides with that in the square-root approach.

5. Chebyshev complete-square block-encoding:

The relation $\lambda_{ij}^{(m)} = \epsilon_i^{(m)} \epsilon_j^{(m)}$ in the double factorization approach allows one to factorize quadratic polynomials into complete squares

$$\hat{f}^{(m)} = \sum_{ij, \sigma \sigma'} \lambda_{ij}^{(m)} \hat{n}_{i\sigma} \hat{n}_{j\sigma'} = \left(\sum_{i, \sigma} \epsilon_i^{(m)} \hat{n}_{i\sigma} \right)^2. \quad (37)$$

Given a fragment with a complete-square structure $\hat{f} = \hat{l}^2$, its implementation can be efficiently done if an efficient implementation of \hat{l} is available^{7,8}, which as shown by Eqs.(30) and (36) is optimal for the case of one-electron operators. Implementation of \hat{f} is done by using the block-encoding of a normalized operator $\hat{l}_n \equiv \hat{l}/\|\hat{l}\|$, followed by the qubitization technique^{6,19}, which implements the Chebyshev polynomial $T_2[\hat{l}_n] = 2\hat{l}_n^2 - \hat{1}$. Thus, by presenting

$$\hat{f} = \frac{\|\hat{l}\|^2}{2} T_2[\hat{l}_n] + \frac{\|\hat{l}\|^2}{2} \hat{1}, \quad (38)$$

this fragment can be implemented with an associated 1-norm cost of $\frac{\|\hat{l}\|^2}{2}$. We will refer to this technique as a complete-square encoding.

Having introduced all LCU decompositions, we now discuss the relation between the square-root technique and complete-square encoding. Both these techniques implement each fragment as a single unitary instead of splitting it to individual reflections, and thus their 1-norm cost is the spectral norm of the fragment. When using the DF technique, the obtained fragments have a complete-square structure [Eq. (37)]. The spectral range, and associated 1-norm for the square-root approach of this fragment is

$$\frac{1}{2} \|\hat{f}_{\text{DF}}^{(m)}\|_\Delta = \frac{1}{2} \left(\max \left\{ \sum_{\lambda_i^{(m)} > 0} \lambda_i^{(m)}, \sum_{\lambda_i^{(m)} < 0} |\lambda_i^{(m)}| \right\} \right)^2. \quad (39)$$

This 1-norm is the same as that obtained with complete-square encoding. Thus, complete-square fragments can be encoded optimally with the lowest possible 1-norm, while for the more general case of $\lambda_{ij}^{(m)} \neq \epsilon_i^{(m)} \epsilon_j^{(m)}$ either the square-root technique can be applied or their $\lambda_{ij}^{(m)}$ can be decomposed into a sum over complete squares.

D. Norm reduction by using symmetry shifts

The idea of using symmetry shifts \hat{S} uses the same rationale as that of shifting the Hamiltonian by $\gamma\hat{1}$: the overall 1-norm of the LCU decomposition can be lowered by decomposing $\hat{H} - \hat{S}$ instead of \hat{H} . By considering an arbitrary symmetry operator \hat{S} for which $[\hat{H}, \hat{S}] = 0$, the time-evolution operator becomes

$$e^{-i\hat{H}t} = e^{-i\hat{S}t} e^{-i(\hat{H}-\hat{S})t}. \quad (40)$$

For a wavefunction that obeys symmetry constraints, $e^{-i\hat{S}t}$ only introduces a phase, making the simulation problem equivalent to the simulation of $\hat{H} - \hat{S}$. In this section we focus on ways to find this shift operator such that the 1-norm of the resulting LCU is lowered. We outline two symmetry shifting procedures that can be applied to fermionic- and qubit-based LCU decompositions. Note that this symmetry shift technique can also improve Trotter methods as well.

1. Shifting fermionic fragments

Since every fragment has its own orbital frame (\hat{U}_m), a symmetry shift is applied independently to each fragment $\hat{f}^{(m)}$ in Eq.(32). The symmetry shift procedure starts by considering a set of symmetries $\mathbb{S} = \{\hat{S}_u\}$, which satisfy conditions $[\hat{S}_u, \hat{S}_v] = [\hat{U}_m \hat{f}^{(m)} \hat{U}_m^\dagger, \hat{S}_u] = 0$, $\forall u, v \in 1, \dots, |\mathbb{S}|$ and $m \in 1, \dots, M$, note that $[\hat{H}, \hat{S}_u] = 0$ follows from these conditions. The symmetries satisfying these constraints are number of electrons with spin

$\alpha(\beta)$: $\hat{N}_{\alpha(\beta)} \equiv \sum_i \hat{n}_{i\alpha(\beta)}$, which are linear combinations of the frequently used number of electrons $\hat{N}_e = \sum_i (\hat{n}_{i\alpha} + \hat{n}_{i\beta})$ and total spin $\hat{S}_z = \frac{1}{2} \sum_i (\hat{n}_{i\alpha} - \hat{n}_{i\beta})$ molecular symmetries. The set of symmetries is defined as we build all possible operators with two-electron representations that are functions of these two symmetries: $\mathbb{S} = \{\hat{N}_\alpha, \hat{N}_\beta, \hat{N}_\alpha^2, \hat{N}_\beta^2, \hat{N}_\alpha \hat{N}_\beta\}$. Other symmetry operators such as \hat{S}^2 and point-group symmetries cannot be represented as polynomials of occupation numbers, rendering them incompatible with the reduction technique we here outline.

The next consideration is how to find the optimal symmetry shift for 1-norm reduction. Given an arbitrary operator \hat{O} , we define the shifted operator

$$\hat{O}(\vec{s}) = \hat{O} - \sum_u s_u \hat{S}_u. \quad (41)$$

where the coefficient vector \vec{s} is a free parameter for the 1-norm minimization of $\hat{O}(\vec{s})$. For the fermionic fragments, each $\hat{f}^{(m)}$ is shifted as

$$\hat{f}^{(m)}(\vec{s}^{(m)}) = \hat{f}^{(m)} - \sum_u s_u^{(m)} \hat{S}_u \quad (42)$$

$$= \sum_{\sigma\sigma', ij} \left(\lambda_{ij}^{(m)} - \left(\sum_u s_u^{(m)} \tau_{i\sigma j\sigma'}^{(u)} \right) \right) \hat{n}_{i\sigma} \hat{n}_{j\sigma'}, \quad (43)$$

where we have written the general form of an occupation number polynomial symmetry as $\hat{S}_u \equiv \sum_{\sigma\sigma'} \sum_{ij} \tau_{i\sigma j\sigma'}^{(u)} \hat{n}_{i\sigma} \hat{n}_{j\sigma'}$, with the tensor $\tau_{i\sigma j\sigma'}^{(u)}$ encoding the coefficients associated with symmetry \hat{S}_u , and used $[\hat{U}_m, \hat{S}_u] = 0$. As shown in Eqs.(30) and (31), each one of these fragments has a two-fold contribution to the total 1-norm: the first one coming from the two-electron fragment, with the second one coming from its associated modification of the one-electron term seen in Eq.(27). Since the second contribution will depend on all the individual shifts, finding shifts that minimize the total 1-norm becomes complicated as all shift parameters have to be optimized simultaneously. Instead we chose a more computationally efficient route, where the optimal shift parameters $\vec{s}^{(m)}$ for each fragment are found by minimizing only the two-electron contribution in Eq.(31) and thus can be found in parallel. When combined with Eq.(42), the 1-norm optimization condition for each shift becomes

$$\vec{s}^{(m)} = \text{argmin}(\vec{s}) \left\{ \frac{1}{4} \sum_{\substack{\sigma\sigma', ij \\ i\sigma \neq j\sigma'}} |\lambda_{ij}^{(m)} - \sum_u s_u \tau_{i\sigma j\sigma'}^{(u)}| \right\}. \quad (44)$$

Appendix C 1 shows an efficient procedure for finding this optimal shift $\vec{s}^{(m)}$. Once the symmetry shifts have been found for each fragment, we can write the Hamiltonian as

$$\hat{H} = \hat{H}_1 + \sum_m \hat{f}^{(m)}(\vec{s}^{(m)}) + \sum_u s_u \hat{S}_u, \quad (45)$$

where we have defined the total shift vector $\vec{s} \equiv \sum_m \vec{s}^{(m)}$. In the same way that a modified one-electron operator \hat{H}'_1 is defined in Eq.(27) and contributes to the 1-norm as in Eq.(30), its shift-dependent version is defined as

$$\hat{H}''_1 \equiv \hat{H}'_1 - \frac{1}{2} \sum_{\sigma\sigma'} \sum_{ij} (\hat{n}_{i\sigma} + \hat{n}_{j\sigma'}) \sum_u s_u \tau_{i\sigma j\sigma'}^{(u)}. \quad (46)$$

A one-electron symmetry shift procedure can now be done for this operator analogously to the fragment shifting procedure that was just outlined, while using only the one-electron symmetries \hat{N}_α and \hat{N}_β . The procedure for doing this one-electron symmetry reduction is shown in Appendix C 2, and yields the optimal vector \vec{r} such that the 1-norm of $\hat{H}''_1(\vec{r}) \equiv \hat{H}'_1 - r_1 \hat{N}_\alpha - r_2 \hat{N}_\beta$ is minimized.

2. Shifting \hat{H}

For the qubit based methods (e.g. anti-commuting grouping technique), the Hamiltonian is never partitioned into fragments and thus only one shift is necessary. Yet, this also means that an occupation number polynomial form is not available, making the application of the fermionic shift technique not feasible. Even though we could optimize the 1-norm of the shifted full Hamiltonian through Eq.(12) by including the symmetry shift in the cost function, this route is computationally expensive as it requires an optimization over $\mathcal{O}(N^4)$ equations. Instead of finding the shift for the full Hamiltonian \hat{H} , we work with an approximate version, \hat{H}_{diag} , which has an occupation number polynomial structure and only requires optimization over $\mathcal{O}(N^2)$ equations. First, \hat{H} can be expressed as a two-electron tensor (for more details see Appendix B):

$$\hat{H} = \sum_{pqrs} \tilde{h}_{pqrs} \hat{E}_q^p \hat{E}_s^r. \quad (47)$$

Then,

$$\hat{H}_{diag} \equiv \sum_{pq} \tilde{h}_{ppqq} \hat{n}_p \hat{n}_q, \quad (48)$$

is introduced as an approximation to \hat{H} . \hat{H}_{diag} has a simple 1-norm

$$\lambda_{diag} = \frac{1}{2} \sum_{pq} |\tilde{h}_{ppqq}| \quad (49)$$

for the associated LCU transformed version, $\hat{n}_p \hat{n}_q \rightarrow (\hat{1} - 2\hat{n}_p \hat{n}_q)$. Since this 1-norm only considers occupation number operators, it can be trivially shifted with the symmetries consisting of occupation number operators in \mathbb{S} . Using the linear programming technique outlined in Appendix C 1, the symmetry shift \vec{s} is found as

$$\vec{s} = \text{argmin}(\{s_u\}) \left\{ \sum_{pq} |\tilde{h}_{ppqq} - \sum_u s_u \tau_{pq}^{(u)}| \right\}, \quad (50)$$

where we have defined the spin-orbital tensor $\tau_{pq}^{(u)}$ associated with \hat{S}_u as $\tau_{pq}^{(u)} \equiv \tau_{i\sigma j\sigma'}^{(u)}$ for $p = i\sigma$ and $q = j\sigma'$. The symmetry shifted Hamiltonian becomes

$$\hat{H}(\vec{s}) = \hat{H} - \sum_u s_u \hat{S}_u, \quad (51)$$

which is subsequently transformed into its qubit representation, where the qubit-based LCU decompositions can be applied.

E. Hamiltonian simulation in the interaction picture

Here, we consider the interaction picture Hamiltonian simulation introduced in Ref. 14. The Hamiltonian is split in two fragments, $\hat{H} = \hat{H}_0 + \hat{H}_R$, where \hat{H}_0 is exactly solvable or fast-forwardable and \hat{H}_R is a residual part. It is beneficial to achieve $\|\hat{H}_0\| \gg \|\hat{H}_R\|$ in this splitting. The simulation of the molecular Hamiltonian then requires the time-dependent simulation of the residual Hamiltonian in the interaction picture, which reduces the overall cost of the simulation.

For selecting \hat{H}_0 we use the CSA approach, by finding the orbital rotation amplitudes $\vec{\theta}$ and occupation number parameters $(\vec{\mu}, \vec{\lambda})$ in

$$\hat{H}_0 = \hat{U}(\vec{\theta}) \left(\sum_{\sigma,i} \mu_i \hat{n}_{i\sigma} + \sum_{\sigma\sigma',i>j} \lambda_{ij} \hat{n}_{i\sigma} \hat{n}_{j\sigma'} \right) \hat{U}^\dagger(\vec{\theta}), \quad (52)$$

to minimize $\|\hat{H} - \hat{H}_0\|$, where the norm is defined as a sum of L_2 norms for one- and two-electron tensors. \hat{H}_0 corresponds to a largest mean-field solvable part²⁶ of \hat{H} .

In the interaction picture, the time-dependent Schrödinger equation is

$$i\partial_t |\psi_I(t)\rangle = \hat{H}_R^{(I)}(t) |\psi_I(t)\rangle, \quad (53)$$

where $|\psi_I(t)\rangle \equiv e^{i\hat{H}_0 t} |\psi(t)\rangle$ and

$$\hat{H}_R^{(I)}(t) = e^{i\hat{H}_0 t} \hat{H}_R e^{-i\hat{H}_0 t}. \quad (54)$$

Simulating the evolution under the full Hamiltonian is thus equivalent to rotating to the interaction frame by $e^{i\hat{H}_0 t}$, doing the simulation with the time-dependent residual $\hat{H}_R^{(I)}(t)$, and rotating back to the Schrödinger frame by $e^{-i\hat{H}_0 t}$.

As shown in Ref. 14, the associated simulation cost for the interaction picture method using a truncated Dyson series is

$$\mathcal{O} \left(\lambda_R t \text{polylog} \left(\frac{\lambda t}{\epsilon} \right) \right) \quad (55)$$

applications of the \hat{H}_R Hamiltonian oracle and of $e^{i\tau\hat{H}_0}$ (with different values of τ), where λ_R is the 1-norm of the LCU decomposition of \hat{H}_R .

III. RESULTS AND DISCUSSION

A. Schrödinger picture

Table I shows the 1-norms obtained for different methods on molecular Hamiltonians. A comparison of each method was made with respect to the simple Pauli product decomposition. The linear fit for each LCU decomposition was done by associating to each molecule two coordinates: x is the 1-norm of the Pauli product LCU, and y is the 1-norm of the considered LCU method. The slope of the linear fit quantifies the average 1-norm reduction of each method with respect to the Pauli product LCU decomposition.

For the qubit-based methods, the orbital rotation scheme presents an improvement with respect to the Pauli product LCU, as expected from the analysis in Ref. 15. This trend is also true for the anti-commuting grouping technique. For all systems, combining the orbital rotation treatment with anti-commuting grouping and/or symmetry shift²⁷ did not present any improvements, we omit these results for brevity. Symmetry shift presented a significant improvement in 1-norm for all systems. It is the best qubit-based method when combined with the anti-commuting grouping, with an average decrease of 1-norm by 42%.

Before discussing the fermionic methods, we would like to emphasize that complete-square encoding will yield the lowest possible 1-norm for fragments with a complete-square structure. Therefore, the square-root 1-norms also correspond to those of DF with complete-square encoding (used in Refs. 7,8). For the symmetry shifted fragments, the complete-square structure is no longer present, and the complete-square encoding cannot be done. We also note that implementing fragments as a single unitary not only reduces the 1-norm, but also the number of unitaries and consequently the number of ancilla qubits. Thus, the square-root technique works as a lower bound for the 1-norm and can be used to know how much the fermionic LCU can be further improved along with providing intuition about the minimal number of ancillary qubits needed. Since the number of ancilla qubits will also depend on the particular implementation of the controlled unitaries^{7,8}, Table I shows $\lceil \log_2 M \rceil$, where M is the number of unitaries in the LCU and the number of ancillas scales with $\mathcal{O}(\lceil \log_2 M \rceil)$.

As shown in Table I, all fermionic methods show a significant improvement with application of symmetry shift. The symmetry-shifted greedy CSA approach with the square-root technique (GCSA-SR) gave lowest 1-norms, with an average reduction of 58%. However, this is an unattainable lower bound. Thus, we highlight methods with the best average gain that use viable implementation methods by employing simple quantum circuits. Before symmetry shift, the best fermionic method is DF with the complete-square encoding, having an average

System	Symmetry shift	$\Delta E/2$	Pauli	OR-Pauli	AC	DF-F	DF-SR	GCSA-F	GCSA-SR
H_2	–	0.82	1.58(4)	1.41(5)	1.41(4)	1.79(5)	1.37(2)	1.40(4)	1.18(2)
	yes	0.57	0.78(4)	–	0.62(4)	0.75(5)	0.75(2)	0.74(4)	0.74(2)
LiH	–	4.93	13.0(10)	12.2(11)	10.2(7)	13.2(10)	9.34(5)	11.0(11)	8.23(5)
	yes	3.62	7.72(10)	–	5.25(7)	8.57(10)	6.61(5)	5.42(11)	4.60(5)
BeH_2	–	9.99	22.8(10)	22.1(12)	18.0(8)	23.8(10)	16.4(5)	19.5(12)	14.4(5)
	yes	7.36	14.4(10)	–	10.2(8)	15.6(10)	13.0(5)	11.1(11)	9.39(5)
H_2O	–	41.9	71.9(11)	63.3(12)	57.2(8)	65.5(11)	53.7(5)	59.1(12)	50.5(5)
	yes	33.1	58.0(11)	–	44.2(8)	42.8(11)	38.4(5)	35.9(12)	31.9(5)
NH_3	–	33.8	67.5(12)	56.8(13)	48.6(9)	58.5(12)	44.7(6)	50.7(13)	40.8(6)
	yes	24.6	55.8(12)	–	37.7(9)	39.9(12)	33.5(6)	31.4(13)	26.7(6)
Linear fit slope	–	0.54 ± 0.03	1	0.87 ± 0.02	0.76 ± 0.02	0.9 ± 0.02	0.71 ± 0.02	0.79 ± 0.02	0.65 ± 0.02
	yes	0.41 ± 0.03	0.8 ± 0.02	–	0.58 ± 0.02	0.6 ± 0.01	0.52 ± 0.01	0.48 ± 0.01	0.42 ± 0.01

TABLE I. 1-norms for molecular Hamiltonian using different LCU decompositions: $\Delta E/2 = (E_{\max} - E_{\min})/2$ is the lowest 1-norm possible; Pauli, Pauli products; AC, anti-commuting Pauli product grouping; OR-Pauli, Pauli products with orbital-rotation optimizing 1-norm; DF, double factorization; GCSA, Greedy CSA decomposition. Symmetry shift procedure is outlined in Sec. IID for both qubit- and fermionic-based methods; $\Delta E/2$ for symmetry shifted case corresponds to qubit-based methods. Suffixes -F and -SR for DF and GCSA correspond to fermionic unitarization and square root unitarization techniques, respectively. The numbers for -SR and complete-square encoding are the same for the non-symmetry shifted DF, and thus only -SR is shown. Values in parenthesis represent $\lceil \log_2(\# \text{ unitaries}) \rceil$, which is associated with the necessary number of ancilla qubits and circuit depth (see Refs. 7,8 for a more detailed discussion). A cut-off threshold of 10^{-6} was used for counting unitaries in fermionic unitarizations. The linear fit was obtained by associating to each molecule two coordinates: x is the 1-norm of the Pauli product LCU, and y is the 1-norm of the considered LCU method. The slope of the linear regression is given with the associated standard error (\pm). Highlights show methods with best scaling that are viable to implement on a quantum computer.

System	$\Delta E/2$	Pauli	AC	OR-Pauli	OR-AC	DF-F	DF-CSE	GCSA-F	GCSA-SR
H_2	0.20	0.30(3)	0.30(3)	0.30(3)	0.30(3)	0.30(3)	0.20(1)	0.20(3)	0.20(1)
LiH	0.80	3.12(10)	1.46(7)	2.50(10)	1.31(7)	1.80(10)	1.40(5)	2.06(11)	1.50(5)
BeH_2	1.00	5.78(10)	2.57(8)	4.16(10)	2.30(8)	4.4(10)	2.89(5)	4.16(12)	2.6(5)
H_2O	2.38	9.18(11)	4.20(8)	7.34(11)	3.68(8)	6.27(11)	4.47(5)	8.05(12)	5.19(6)
NH_3	3.02	17.2(13)	6.56(9)	10.1(13)	4.85(9)	9.43(12)	6.41(6)	11.2(13)	7.14(6)
Linear fit slope	0.04 ± 0.003	0.19 ± 0.03	0.08 ± 0.01	0.13 ± 0.01	0.06 ± 0.01	0.12 ± 0.02	0.08 ± 0.01	0.14 ± 0.01	0.09 ± 0.01

TABLE II. Same as Table I, but for residual Hamiltonian \hat{H}_R : OR-AC, orbital rotation scheme with subsequent anti-commuting Pauli product grouping; DF-CSE, double factorization with complete-square encoding, which has the same numbers as DF-SR and the latter is not shown. The linear fit is calculated with respect to the Pauli product LCU for \hat{H} .

decrease of the 1-norm by 29%. When the symmetry shift was applied, all methods presented a significant improvement, having the largest reduction of 52% for the greedy CSA with the fermionic reflections (GCSA-F) method.

Even though the CSA decomposition is a more general ansatz than DF, the greedy algorithm used in CSA for finding the fragments is heuristic and sacrifices some flexibility of a full optimization in exchange for computational efficiency. This makes the number of fragments and as a result the number of ancilla qubits appearing in GCSA larger than those in DF.

It should also be noted that doing the GCSA decomposition is a computationally expensive process compared to DF; these methods respectively require a non-linear optimization and a Cholesky decomposition. When considering the symmetry shift, both anti-commuting and DF with a fermionic unitarization methods present the best improvement for 1-norm while having the lowest classical pre-processing cost. These methods show an improvement of 42% and 40% respectively, offering a sig-

nificant improvement over all methods without symmetry shift. The anti-commuting grouping also requires the lowest number of ancilla qubits out of all methods with a viable implementation.

Although both DF and CSA decompositions could be done over the full Hamiltonian by representing it as a single two-electron operator (see Appendix B), separating the one- and two-electron terms yields a very significant improvement of the 1-norm, while also allowing for manipulations to be done directly on spatial orbitals (as opposed to spin-orbitals), which greatly lowers the classical pre-processing cost of the decompositions.

Finally, we discuss how our results compare to the 1-norm lower bound $\Delta E/2$. When not considering symmetry shift, DF-SR lowered the 1-norm by 63% of the possible reduction, while with symmetry shift GCSA-F captured 88%. When dealing with symmetry shifted molecular Hamiltonians, GCSA-F obtains a 1-norm that is very close to the lower bound, placing it as an almost optimal decomposition method.

B. Interaction picture

Table II provides results for the same LCU method but in the interaction picture. The linear fit results are also obtained by comparing the 1-norms with respect to the Pauli product LCU 1-norm of the molecular Hamiltonian in the Schrödinger picture.

Here, performing the symmetry shift does not yield any significant improvements on any of the methods and thus is not shown in Table II. This can be attributed to an implicit inclusion of any symmetry shift of \hat{H}_0 in its μ_i and λ_{ij} coefficients: $\hat{H}_0 - \sum_u s_u \hat{S}_u \equiv \hat{U}(\vec{\theta}) \left(\sum_{\sigma,i} \tilde{\mu}_i(\vec{s}) \hat{n}_{i\sigma} + \sum_{\sigma\sigma',i>j} \tilde{\lambda}_{ij}(\vec{s}) \hat{n}_{i\sigma} \hat{n}_{j\sigma'} \right) \hat{U}^\dagger(\vec{\theta})$ since $[\hat{S}_u, \hat{U}(\vec{\theta})] = 0$ and \hat{S}_u is a polynomial of occupation numbers. Without symmetry shifts, DF fragments are complete squares, which enables the complete-square encoding. This makes the DF technique the most optimal fermionic method, with an average 1-norm decrease of 92% with respect to the Pauli product LCU of the molecular Hamiltonian. Surprisingly, the results from GCSA are not consistently better than those of DF. We attribute this to the heuristic nature of the greedy optimization. DF is thus a better alternative than GCSA for decomposing \hat{H}_R , presenting a greater 1-norm reduction, smaller number of fragments, and a lower classical pre-processing cost.

For the qubit-based methods, the anti-commuting grouping presented the greatest 1-norm reduction. We observed that applying the orbital rotation scheme further improved the results when combined with the anti-commuting grouping. The combination of these techniques yielded an average 1-norm reduction of 94%, while without the orbital rotation scheme the anti-commuting grouping presented an average decrease of 92%. As opposed to the molecular Hamiltonian case, the orbital rotation gave an additional improvement for \hat{H}_R . This is due to the structure of \hat{H}_R that is obtained after a greedy procedure for finding \hat{H}_0 , as opposed to \hat{H} that comes from the molecular integrals.

IV. CONCLUSION

We have presented a wide set of techniques for performing the LCU decomposition of molecular Hamiltonians, using the associated 1-norm of the decomposition as the main figure of merit. The greatest 1-norm reduction was observed for the interaction picture methodology combined with the orbital rotation scheme and anti-commuting Pauli products grouping, with an average 1-norm decrease of 94% with respect to the Pauli product LCU of the molecular Hamiltonian \hat{H} . All methods that work with the residual \hat{H}_R of the interaction picture greatly improved the performance over decomposing \hat{H} , decreasing the 1-norm by an

order of magnitude. However, the interaction picture methodology requires a time-dependent simulation method, rendering it incompatible with some simulation techniques such as qubitization (although recent work has shown that qubitization can be made to work for restricted families of time-dependent Hamiltonians, existing results preclude the interaction picture²⁸). For the time-independent case, the symmetry shift technique here introduced can be employed, which yields a significant decrease of the 1-norm when compared with commonly used techniques⁷ and can be included in a tensor hypercontraction framework^{8,29}. Even though we only used symmetry shifts that can be written as functions of occupation number operators such as \hat{N}_e and \hat{S}_z , the results presented here provide an incentive for exploring more symmetries with different structures, such as \hat{S}^2 and molecular point-group symmetries. Finally, we have found tight bounds for the 1-norm of an arbitrary LCU, with the most efficient decomposition shown here being close to the lower bound.

Overall, we presented different methodologies for reducing the LCU 1-norm cost of molecular Hamiltonians, with significant improvements that can be applied both for time-independent⁶ and time-dependent^{9,14} simulation methods. We expect our results to be of use for any methodology that uses LCU decomposition of molecular Hamiltonians.

ACKNOWLEDGEMENTS

I.L. is grateful to Tzu-Ching Yen for helpful discussions and to Luis Martínez-Martínez, Joshua T. Cantin, and Seonghoon Choi for their comments on the manuscript, and is supported by the funding of the Anoush Khoshkish Graduate Research Scholarship in Chemistry. A.F.I. acknowledges financial support from the Google Quantum Research Program, Zapata Computing, and the Natural Sciences and Engineering Research Council of Canada. N.W. acknowledges funding from the Google Quantum Research Program, the Natural Sciences and Engineering Research Council of Canada and N.W.'s theoretical work on this project was supported by the U.S. Department of Energy, Office of Science, National Quantum Information Science Research Centers, Co-Design Center for Quantum Advantage under contract number DE-SC0012704.

Appendix A: Proof of the lowest 1-norm theorem

Theorem 1 (1-norm bound). *For a bounded hermitian operator \hat{H} , all its possible LCU decompositions have an associated 1-norm which is lower bounded by $\Delta E/2 \equiv (E_{\max} - E_{\min})/2$, where $E_{\max}(E_{\min})$ is the highest (lowest) eigenvalue of \hat{H} .*

Proof of Theorem 1. The construction of a LCU that

achieves the lower bound is given in Sec. II B of the main text. We now proceed to show, by contradiction, that no LCU with a lower 1-norm can be found.

Let us assume that it is possible to construct $\hat{H} = \sum_k u_k \hat{U}_k$ such that $\sum_k |u_k| < \Delta E/2$. Denoting $|\psi_{\max}\rangle (|\psi_{\min}\rangle)$ the maximum (minimum) eigenvectors, we have

$$\begin{aligned} \langle \psi_{\max} | \sum_k u_k \hat{U}_k | \psi_{\max} \rangle &= E_{\max} \\ \langle \psi_{\min} | \sum_k u_k \hat{U}_k | \psi_{\min} \rangle &= E_{\min}. \end{aligned} \quad (\text{A1})$$

We therefore have that $\Delta E/2$ can be bounded above by

$$\begin{aligned} \frac{\Delta E}{2} &= \frac{1}{2} \left(\langle \psi_{\max} | \sum_k u_k \hat{U}_k | \psi_{\max} \rangle - \langle \psi_{\min} | \sum_k u_k \hat{U}_k | \psi_{\min} \rangle \right) \\ &\leq \sum_k |u_k| < \frac{\Delta E}{2}, \end{aligned} \quad (\text{A2})$$

where we have used the triangle inequality and the fact that $|\langle \psi | \hat{U} | \psi \rangle| \leq 1$ for any unitary \hat{U} and wavefunction $|\psi\rangle$. This is a contradiction, thus $\sum_k |u_k| \geq \Delta E/2$ as claimed. \square

Appendix B: One-electron term transformations

Due to idempotency of occupation operator terms, $(E_{i\sigma}^{i\sigma})^2 = E_{i\sigma}^{i\sigma}$, one-electron terms can be transformed to two-electron terms and vice versa. This section shows how these transformations can be done for general two-electron operators.

1. Transforming to two-electron terms

We start by showing how to combine one- and two-electron terms into a sum of two-electron terms. An arbitrary operator with spin-orbit symmetry can be written as

$$\hat{O} = \hat{O}_1 + \hat{O}_2 \quad (\text{B1})$$

$$= \sum_{\sigma} \sum_{ij} o_{ij} \hat{E}_{j\sigma}^{i\sigma} + \sum_{\sigma\sigma'} \sum_{ijkl} o_{ijkl} \hat{E}_{j\sigma}^{i\sigma} \hat{E}_{l\sigma'}^{k\sigma'} \quad (\text{B2})$$

We note that each o_{ij} is multiplied by two excitation operators $\hat{E}_{j\sigma}^{i\sigma}$ with $\sigma \in (\alpha, \beta)$, while each o_{ijkl} is multiplied by four operators $(\alpha\alpha, \alpha\beta, \beta\alpha, \beta\beta)$. Because of this, combining both operators requires to change from a (spatial) orbital representation into the spin-orbital one; the combined two-electron operator will have different components for $(\alpha\alpha, \beta\beta)$ and $(\alpha\beta, \beta\alpha)$. We now transform the one-electron term into a two-electron operator, noting that several different transformations can be done

here. We use the one that maintains a symmetric two-electron tensor since this property makes computational manipulations more efficient:

$$\hat{O}_1 = \hat{U} \sum_{\sigma} \sum_i \mu_i \hat{n}_{i\sigma} \hat{U}^{\dagger} \quad (\text{B3})$$

$$= \hat{U} \sum_{\sigma} \sum_i \mu_i \hat{n}_{i\sigma} \hat{n}_{i\sigma} \hat{U}^{\dagger} \quad (\text{B4})$$

$$= \sum_{\sigma} \sum_{ijkl} \tilde{o}_{ijkl} \hat{E}_{j\sigma}^{i\sigma} \hat{E}_{l\sigma}^{k\sigma}, \quad (\text{B5})$$

with

$$\tilde{o}_{ijkl} = \sum_m \mu_m U_{im} U_{jm} U_{km} U_{lm}, \quad (\text{B6})$$

for $\hat{U} \equiv \sum_{\sigma} \sum_{ij} U_{ij} \hat{E}_{j\sigma}^{i\sigma}$. The combined two-electron tensor is o_{pqrs} , where

$$\begin{aligned} \hat{O} &= \sum_{\sigma} \sum_{ijkl} (\tilde{o}_{ijkl} + o_{ijkl}) \hat{E}_{j\sigma}^{i\sigma} \hat{E}_{l\sigma}^{k\sigma} + \sum_{\sigma \neq \sigma'} \sum_{ijkl} o_{ijkl} \hat{E}_{j\sigma}^{i\sigma} \hat{E}_{l\sigma'}^{k\sigma'} \\ &\equiv \sum_{pqrs} o_{pqrs} \hat{E}_q^p \hat{E}_s^r. \end{aligned} \quad (\text{B7})$$

$$\equiv \sum_{pqrs} o_{pqrs} \hat{E}_q^p \hat{E}_s^r. \quad (\text{B8})$$

2. Separating one-electron terms

Here we show how one-electron terms can be separated from the two-electron tensor, which is used to connect the fermionic and qubit representations. This is necessary for writing the 1-norm of qubit-based methods as a function of the molecular integrals, and also for a more efficient sorted-insertion algorithm that does not require any fermion to qubit mappings. This methodology is introduced in Ref. 15, only the final result and key steps are presented here. We start from a general two-electron operator with spin-symmetry, as seen in Eq.(B2). For the next step, we switch to the Majorana representation, where fermionic operators are mapped into Majorana operators as

$$\hat{\gamma}_{j\sigma,0} = \hat{a}_{j\sigma} + \hat{a}_{j\sigma}^{\dagger} \quad (\text{B9})$$

$$\hat{\gamma}_{j\sigma,1} = -i(\hat{a}_{j\sigma} - \hat{a}_{j\sigma}^{\dagger}), \quad (\text{B10})$$

which have the well-known algebraic relations:

$$\{\hat{\gamma}_{p,n}, \hat{\gamma}_{q,m}\} = 2\delta_{pq}\delta_{nm}\hat{1} \quad (\text{B11})$$

$$\hat{\gamma}_{p,n}^{\dagger} = \hat{\gamma}_{p,n} \quad (\text{B12})$$

$$\hat{\gamma}_{p,n}^2 = \hat{1}, \quad (\text{B13})$$

for $n, m = 0, 1$. By transforming the fermionic operators into Majoranas, after proper manipulations, \hat{O} can be

written as

$$\begin{aligned}
\hat{O} = & \left(\sum_i o_{ii} + \sum_{ij} o_{ijjj} \right) \hat{1} \\
& + \frac{i}{2} \sum_{\sigma} \sum_{ij} \left(o_{ij} + 2 \sum_k o_{ijkk} \right) \hat{\gamma}_{i\sigma,0} \hat{\gamma}_{j\sigma,1} \\
& - \frac{1}{4} \sum_{\sigma \neq \sigma'} \sum_{ijkl} o_{ijkl} \hat{\gamma}_{i\sigma,0} \hat{\gamma}_{j\sigma,1} \hat{\gamma}_{k\sigma',0} \hat{\gamma}_{l\sigma',1} \\
& - \frac{1}{2} \sum_{\sigma} \sum_{i>k, l>j} (o_{ijkl} - o_{ilkj}) \hat{\gamma}_{i\sigma,0} \hat{\gamma}_{j\sigma,1} \hat{\gamma}_{k\sigma,0} \hat{\gamma}_{l\sigma,1}.
\end{aligned} \tag{B14}$$

In this equation, all terms with a product of 2 Majorana operators correspond to the one-electron terms, while terms with 4 Majorana operators correspond to two-electron terms. This representation thus allows for the analytical separation of the one-electron terms that are present in the two-electron tensor. Finally, we note that each resulting Majorana product will map to an individual Pauli product when using fermion to qubit mappings such as Jordan-Wigner or Bravyi-Kitaev.

Appendix C: Finding the optimal symmetry shift for 1-norm minimization

In this section we present procedures for finding the coefficient vector associated with the symmetry shift procedure in Sec. IID, both for the one- and two-electron cases.

1. Two-electron symmetry reduction

For finding the symmetry shift of two-electron operators, we here present a linear programming routine that minimizes the 1-norm and is computationally efficient.

Our objective is to minimize the 1-norm appearing in Eq.(44), which can be written succinctly as

$$\min_{\vec{s}} \sum_{\nu=1}^{|C|} |\lambda_{\nu} - \sum_{u=1}^{|S|} s_u \tau_{\nu}^{(u)}|. \tag{C1}$$

In the above equation, vector $\vec{\lambda}$ collects the diagonal elements of the two-electron tensor that appear in the array of Cartan operators $C = \{\hat{n}_p \hat{n}_q \mid p \geq q\} \equiv \{\hat{C}_{\nu} \mid \nu = 1, \dots, |C|\}$. The vectors we use for this notation run over $p \geq q$ in the same order as C , with the number of elements $|C| = n(n+1)/2$. This also defines the $\vec{\tau}^{(u)}$ vectors, which represent the symmetry operators: $\hat{S}_u = \sum_{\nu=1}^{|C|} \tau_{\nu}^{(u)} \hat{C}_{\nu}$. We here use the symmetry operators from the two-electron symmetry set $S = \{\hat{N}_{\alpha}^2, \hat{N}_{\beta}^2, \hat{N}_{\alpha} \hat{N}_{\beta}\}$. For these symmetries, the $\vec{\tau}^{(u)}$ elements are either 1 or 0, indicating Cartan elements that

either appear or not in a particular symmetry operator. s_u is the symmetry shift for each operator, which is the parameter we want to optimize.

We used a linear programming technique to find \vec{s} efficiently while directly minimizing the 1-norm. To this end, we need to transform the sum of absolute values in the 1-norm cost function into a sum of linear parameters. We achieve this by introducing a new set of auxiliary parameters equivalent to the absolute value functions that appear in the 1-norm. The minimization procedure is subject to constraints that satisfy the absolute value conditions. For the 1-norm linearization, let us begin with introducing the auxiliary vector \vec{t} and re-write the objective function as

$$\begin{aligned}
& \min_{\vec{s}} \sum_{\nu} t_{\nu}(\vec{s}) \\
& \text{subject to} \quad t_{\nu}(\vec{s}) = \sum_{\nu} |\lambda_{\nu} - \sum_u s_u \tau_{\nu}^{(u)}|.
\end{aligned} \tag{C2}$$

The absolute value constraints can be written as

$$\sum_u s_u \tau_{\nu}^{(u)} - \lambda_{\nu} \leq t_{\nu} \tag{C3}$$

and

$$-\sum_u s_u \tau_{\nu}^{(u)} + \lambda_{\nu} \leq t_{\nu} \tag{C4}$$

We can now write the final form for the 1-norm minimization problem:

$$\begin{aligned}
& \min_{\{\vec{s}, \vec{t}\}} \sum_{\nu} t_{\nu} \\
& \text{subject to} \quad \begin{pmatrix} \underline{\tau} & -\underline{1} \\ -\underline{\tau} & -\underline{1} \end{pmatrix} \begin{pmatrix} \vec{s} \\ \vec{t} \end{pmatrix} \leq \begin{pmatrix} \vec{\lambda} \\ -\vec{\lambda} \end{pmatrix},
\end{aligned} \tag{C5}$$

where we have defined the matrix $\underline{\tau}$ such that the product $(\underline{\tau} \times \vec{s})_{\nu} \equiv \sum_u s_u \tau_{\nu}^{(u)}$, and the inequality runs over each index $\nu \in \{1, \dots, |C|\}$. The above minimization problem is linear programmable and lets us efficiently find the global minimum of the 1-norm of the objective function. Moreover, the $\underline{\tau}$ matrix helps to avoid storing in memory the full two-electron tensors of symmetry operators, which reduces the memory demand significantly. We used the high global minimization algorithm³⁰ for our numerical calculations.

2. One-electron symmetry reduction

In this section we review the method for finding the optimal symmetry shift minimizing the 1-norm of the one-electron term \hat{H}_1'' shown in Eq.(48). This method optimizes a two-dimensional real vector \vec{r} , such that the resulting 1-norm of the operator $\hat{H}_1''(\vec{r}) \equiv \hat{H}_1'' - r_1 \hat{N}_{\alpha} -$

$r_2 \hat{N}_\beta$ is minimized. This requires a diagonalization, as shown in Eq.(28), of the full $\hat{H}_1''(\vec{r})$ operator for each \vec{r} :

$$\hat{H}_1''(\vec{r}) = \hat{U}_{\vec{r}} \sum_{\sigma} \sum_i \mu_{i\sigma}(\vec{r}) \hat{n}_{i\sigma} \hat{U}_{\vec{r}}^\dagger, \quad (\text{C6})$$

with the resulting 1-norm

$$\lambda_1(\vec{r}) = \frac{1}{2} \sum_{\sigma} \sum_i |\mu_{i\sigma}(\vec{r})|. \quad (\text{C7})$$

A non-linear optimization package is then used to find the optimal \vec{r} such that $\lambda_1(\vec{r})$ is minimized.

Appendix D: Molecular geometries and computational details

In this section we write down all details necessary for numerical reproducibility. Our code is available at <https://github.com/iloaiza/TBFrags>.

For the CSA decompositions of the two-electron tensor, the cost function was chosen as the 2-norm of $\Delta \hat{H} \equiv \sum_{\sigma\sigma'} \sum_{ijkl} b_{ijkl} \hat{E}_{j\sigma}^{i\sigma} \hat{E}_{l\sigma'}^{k\sigma'}$:

$$\|\Delta \hat{H}\|_2 \equiv \sum_{ijkl} |b_{ijkl}|^2, \quad (\text{D1})$$

considering the decomposition finished when this norm is below a tolerance of 2.5×10^{-6} . All non-linear optimizations were done using the Julia Optim.jl package³¹, using the BFGS algorithm³² with the default tolerance. Linear programming routines were done using the SciPy package³³; special emphasis is placed on using a SciPy version $\geq 1.9.0$ since older versions do not consistently achieve the global minimum.

1. Molecular Hamiltonians

All molecular Hamiltonians were generated using the PySCF package^{34–36} and the Openfermion library³⁷, using a minimal STO-3G basis^{3,38} and the Jordan-Wigner transformation²¹. The nuclear geometries for the Hamiltonians are:

- R(H – H) = 1Å for H₂
- R(Li – H) = 1Å for LiH
- R(Be – H) = 1Å with a collinear atomic arrangement for BeH₂
- R(O – H) = 1Å with angle $\angle\text{HOH} = 107.6^\circ$ for H₂O
- R(N – H) = 1Å with $\angle\text{HNN} = 107^\circ$ for NH₃

- ¹D. S. Abrams and S. Lloyd, “Quantum algorithm providing exponential speed increase for finding eigenvalues and eigenvectors,” *Phys. Rev. Lett.* **83**, 5162–5165 (1999).
- ²A. Y. Kitaev, “Quantum measurements and the abelian stabilizer problem,” *arXiv* (1995), 10.48550/ARXIV.QUANT-PH/9511026.
- ³A. Szabo and N. Ostlund, *Modern Quantum Chemistry: Introduction to Advanced Electronic Structure Theory*, Dover Books on Chemistry (Dover Publications, 1996).
- ⁴Representing the Hamiltonian using only excitation operators is usually referred to as chemists’ notation. This entails a modification to the one-electron tensor with respect to physicists’ notation, which uses normal-ordered operators of the form $\hat{a}_p^\dagger \hat{a}_q^\dagger \hat{a}_r \hat{a}_s$. Our notation is related to the electronic integrals by $\tilde{g}_{ijkl} = \frac{1}{2} \int \int d\vec{r}_1 d\vec{r}_2 \frac{\phi_i^*(\vec{r}_1) \phi_j(\vec{r}_1) \phi_k(\vec{r}_2) \phi_l^*(\vec{r}_2)}{|\vec{r}_1 - \vec{r}_2|}$ and $\tilde{h}_{ij} = -\sum_k \tilde{g}_{ikkj} + \int d\vec{r} \phi_i^*(\vec{r}) \left(-\frac{\nabla^2}{2} - \sum_N \frac{Z_N}{|\vec{r} - \vec{r}_N|} \right) \phi_j(\vec{r})$, with $\phi_i(\vec{r})$ the one-particle electronic basis functions, and Z_N/\vec{r}_N the charge/position of nucleus N .
- ⁵M. Suzuki, “General theory of fractal path integrals with applications to many-body theories and statistical physics,” *Journal of Mathematical Physics* **32**, 400–407 (1991), <https://doi.org/10.1063/1.529425>.
- ⁶D. W. Berry, C. Gidney, M. Motta, J. McClean, and R. Babbush, *Quantum* **3** (2019), 10.22331/q-2019-12-02-208.
- ⁷V. von Burg, G. H. Low, T. Haner, D. Steiger, M. Reiher, M. Roetteler, and M. Troyer, *arXiv* (2020), 2007.14460.
- ⁸J. Lee, D. W. Berry, C. Gidney, W. J. Huggins, J. R. McClean, N. Wiebe, and R. Babbush, “Even more efficient quantum computations of chemistry through tensor hypercontraction,” *PRX Quantum* **2** (2021), 10.1103/prxquantum.2.030305.
- ⁹A. M. Childs and N. Wiebe, “Hamiltonian simulation using linear combinations of unitary operations,” *Quantum Info. Comput.* **12**, 901–924 (2012).
- ¹⁰E. Campbell, “Random compiler for fast Hamiltonian simulation,” *Phys. Rev. Lett.* **123**, 070503 (2019).
- ¹¹I. D. Kivlichan, C. E. Granade, and N. Wiebe, “Phase estimation with randomized Hamiltonians,” *arXiv* (2019), 10.48550/ARXIV.1907.10070.
- ¹²A. M. Childs, Y. Su, M. C. Tran, N. Wiebe, and S. Zhu, “Theory of trotter error with commutator scaling,” *Physical Review X* **11**, 011020 (2021).
- ¹³J. Haah, M. B. Hastings, R. Kothari, and G. H. Low, “Quantum algorithm for simulating real time evolution of lattice Hamiltonians,” *SIAM Journal on Computing*, FOCS18–250 (2021).
- ¹⁴G. H. Low and N. Wiebe, “Hamiltonian simulation in the interaction picture,” (2019), [arXiv:1805.00675](https://arxiv.org/abs/1805.00675) [quant-ph].
- ¹⁵E. Koridon, S. Yalouz, B. Senjean, F. Buda, T. E. O’Brien, and L. Visscher, “Orbital transformations to reduce the 1-norm of the electronic structure Hamiltonian for quantum computing applications,” *Physical Review Research* **3** (2021), 10.1103/physrevresearch.3.033127.
- ¹⁶A. F. Izmaylov, T.-C. Yen, R. A. Lang, and V. Verteletskyi, “Unitary partitioning approach to the measurement problem in the variational quantum eigensolver method,” *Journal of Chemical Theory and Computation* **16**, 190–195 (2020), PMID: 31747266, <https://doi.org/10.1021/acs.jctc.9b00791>.
- ¹⁷D. W. Berry, A. M. Childs, Y. Su, X. Wang, and N. Wiebe, “Time-dependent Hamiltonian simulation with l_1 -norm scaling,” *Quantum* **4**, 254 (2020).
- ¹⁸D. W. Berry, A. M. Childs, R. Cleve, R. Kothari, and R. D. Somma, “Simulating Hamiltonian dynamics with a truncated Taylor series,” *Phys. Rev. Lett.* **114**, 090502 (2015).
- ¹⁹G. H. Low and I. L. Chuang, “Hamiltonian simulation by qubitization,” *Quantum* **3**, 163 (2019).
- ²⁰A. Gilyén, Y. Su, G. H. Low, and N. Wiebe, “Quantum singular value transformation and beyond: exponential improvements for quantum matrix arithmetics,” in *Proceedings of the 51st Annual ACM SIGACT Symposium on Theory of Computing* (2019) pp. 193–204.

- ²¹E. Wigner and P. Jordan, “Über das paulische äquivalenzverbot,” *Z. Phys* **47**, 631 (1928).
- ²²S. B. Bravyi and A. Y. Kitaev, “Fermionic quantum computation,” *Annals of Physics* **298**, 210–226 (2002).
- ²³J. T. Seeley, M. J. Richard, and P. J. Love, “The Bravyi-Kitaev transformation for quantum computation of electronic structure,” *The Journal of chemical physics* **137**, 224109 (2012).
- ²⁴A. Tranter, S. Sofia, J. Seeley, M. Kaicher, J. McClean, R. Babbush, P. V. Coveney, F. Mintert, F. Wilhelm, and P. J. Love, “The Bravyi-Kitaev transformation: Properties and applications,” *International Journal of Quantum Chemistry* **115**, 1431–1441 (2015).
- ²⁵T.-C. Yen and A. F. Izmaylov, “Cartan subalgebra approach to efficient measurements of quantum observables,” *PRX Quantum* **2** (2021), 10.1103/prxquantum.2.040320.
- ²⁶A. F. Izmaylov and T.-C. Yen, “How to define quantum mean-field solvable Hamiltonians using Lie algebras,” *Quantum Science and Technology* **6**, 044006 (2021).
- ²⁷Performing the orbital rotation scheme after a symmetry shift requires a slightly different treatment to the one presented here since the orbital rotation is now done on a two-electron tensor in spin-orbitals that has both the one- and two-electron terms, as shown in Appendix B. As such, the representation using Majorana operators uses a different fermionic tensor than the ones shown in Ref. 15 and Appendix B. The details of this scheme are not included here since it does not present any significant improvements.
- ²⁸J. Watkins, N. Wiebe, A. Roggero, and D. Lee, “Time-dependent Hamiltonian simulation using discrete clock constructions,” *arXiv preprint arXiv:2203.11353* (2022).
- ²⁹Including spin-symmetry after symmetry shift so that decompositions can be made on tensors running over spacial-orbitals, and not spin-orbitals, is necessary if classical pre-processing is to remain efficient. Orthonormality of the tensor hypercontraction orbitals also needs to be enforced for the symmetry shift to be applied directly on the contracted tensors. However, these considerations are outside the scope of this work.
- ³⁰Q. Huangfu and J. Hall, “Parallelizing the dual revised simplex method,” *Mathematical Programming Computation* **10** (2018), 10.1007/s12532-017-0130-5.
- ³¹P. K. Mogensen and A. N. Riseth, “Optim: A mathematical optimization package for Julia,” *Journal of Open Source Software* **3**, 615 (2018).
- ³²R. Fletcher, *Practical Methods of Optimization* (Wiley, 2013).
- ³³P. Virtanen, R. Gommers, T. E. Oliphant, M. Haberland, T. Reddy, D. Cournapeau, E. Burovski, P. Peterson, W. Weckesser, J. Bright, S. J. van der Walt, M. Brett, J. Wilson, K. J. Millman, N. Mayorov, A. R. J. Nelson, E. Jones, R. Kern, E. Larson, C. J. Carey, Í. Polat, Y. Feng, E. W. Moore, J. VanderPlas, D. Laxalde, J. Perktold, R. Cimrman, I. Henriksen, E. A. Quintero, C. R. Harris, A. M. Archibald, A. H. Ribeiro, F. Pedregosa, P. van Mulbregt, and SciPy 1.0 Contributors, “SciPy 1.0: Fundamental Algorithms for Scientific Computing in Python,” *Nature Methods* **17**, 261–272 (2020).
- ³⁴Q. Sun, “Libcint: An efficient general integral library for gaussian basis functions,” *Journal of Computational Chemistry* **36**, 1664–1671 (2015), <https://onlinelibrary.wiley.com/doi/pdf/10.1002/jcc.23981>.
- ³⁵Q. Sun, T. C. Berkelbach, N. S. Blunt, G. H. Booth, S. Guo, Z. Li, J. Liu, J. D. McClain, E. R. Sayfutyarova, S. Sharma, S. Wouters, and G. K.-L. Chan, “Pyscf: the python-based simulations of chemistry framework,” *WIREs Computational Molecular Science* **8**, e1340 (2018), <https://wires.onlinelibrary.wiley.com/doi/pdf/10.1002/wcms.1340>.
- ³⁶Q. Sun, X. Zhang, S. Banerjee, P. Bao, M. Barbry, N. S. Blunt, N. A. Bogdanov, G. H. Booth, J. Chen, Z.-H. Cui, J. J. Eriksen, Y. Gao, S. Guo, J. Hermann, M. R. Hermes, K. Koh, P. Koval, S. Lehtola, Z. Li, J. Liu, N. Mardirossian, J. D. McClain, M. Motta, B. Mussard, H. Q. Pham, A. Pulkin, W. Purwanto, P. J. Robinson, E. Ronca, E. R. Sayfutyarova, M. Scheurer, H. F. Schurkus, J. E. T. Smith, C. Sun, S.-N. Sun, S. Upadhyay, L. K. Wagner, X. Wang, A. White, J. D. Whitfield, M. J. Williamson, S. Wouters, J. Yang, J. M. Yu, T. Zhu, T. C. Berkelbach, S. Sharma, A. Y. Sokolov, and G. K.-L. Chan, “Recent developments in the pyscf program package,” *The Journal of Chemical Physics* **153**, 024109 (2020), <https://doi.org/10.1063/5.0006074>.
- ³⁷J. R. McClean, N. C. Rubin, K. J. Sung, I. D. Kivlichan, X. Bonet-Monroig, Y. Cao, C. Dai, E. S. Fried, C. Gidney, B. Gimby, P. Gokhale, T. Häner, T. Hardikar, V. Havlíček, O. Higgott, C. Huang, J. Izaac, Z. Jiang, X. Liu, S. McArdle, M. Neeley, T. O’Brien, B. O’Gorman, I. Ozfidan, M. D. Radin, J. Romero, N. P. D. Sawaya, B. Senjean, K. Setia, S. Sim, D. S. Steiger, M. Steudtner, Q. Sun, W. Sun, D. Wang, F. Zhang, and R. Babbush, “OpenFermion: the electronic structure package for quantum computers,” *Quantum Science and Technology* **5**, 034014 (2020).
- ³⁸W. J. Hehre, R. F. Stewart, and J. A. Pople, “Self-consistent molecular-orbital methods. I. Use of Gaussian expansions of Slater-type atomic orbitals,” *The Journal of Chemical Physics* **51**, 2657–2664 (1969), <https://doi.org/10.1063/1.1672392>.